HHS Public Access

Author manuscript

Eur J Neurosci. Author manuscript; available in PMC 2021 December 01.

Published in final edited form as:

Eur J Neurosci. 2020 December ; 52(12): 4824–4839. doi:10.1111/ejn.15027.

Comparative analyses of transgene expression patterns after intra-striatal injections of rAAV2-retro in rats and rhesus monkeys: a light and electron microscopic study

Daniel L. Albaugh[1,2], **Yoland Smith**[1,2,3], **Adriana Galvan**[1,2,3]

[1]Division of Neuropharmacology and Neurological Disorders, Yerkes National Primate Research Center, Emory University, Atlanta, GA, USA

[2]Udall Center of Excellence for Parkinson's Disease Research, Atlanta, GA, USA

[3]Department of Neurology, School of Medicine, Emory University, Atlanta, GA, USA

Abstract

Retrogradely-transducing viral vectors are versatile tools for anatomical and functional interrogations of neural circuits. These vectors can be applied in nonhuman primates (NHPs), powerful model species for neuroscientific studies with limited genetic tractability, but limited data is available regarding the tropism and transgene expression patterns of such viruses after injections in NHP brains. Consequently, NHP researchers must often rely on related data available from other species for experimental planning. To evaluate the suitability of rAAV2-retro in the NHP basal ganglia, we studied the transgene expression patterns at the light and electron microscope level after injections of rAAV2-retro vector encoding the opsin Jaws conjugated to a green fluorescent protein (GFP) in the putamen of rhesus macaques. For inter-species comparison, we injected the same vector in the rat dorsal striatum. In both species, GFP expression was observed in numerous cortical and subcortical regions with known striatal projections. However, important inter-species differences in pathway transduction were seen, including labeling of the intralaminar thalamostriatal projection in rats, but not monkeys. Electron microscopic ultrastructural observations within the basal ganglia revealed GFP labeling in both postsynaptic dendrites and presynaptic axonal terminals; the latter likely derived from anterograde transgene transport in neurons. that project to the striatum, and from collaterals of these neurons. Our results suggest that certain neural pathways may be refractory to transduction by retrograde vectors in a species-specific manner, highlighting the need for caution when determining the suitability of a retrograde vector for NHP studies based solely on rodent data.

Keywords

Viral Vectors; Striatum; Primate; Electron Microscopy; connectome; retrograde transduction; thalamostriatal; corticostriatal; subthalamic nucleus

Corresponding Author: Daniel L. Albaugh.

Introduction.

Viruses with retrograde transport properties provide an efficient means for selective genetic targeting of neurons based on anatomical projection patterns (Soudais *et al.*, 2001; Hollis II *et al.*, 2008; Kato *et al.*, 2011; Nassi *et al.*, 2015; Tervo *et al.*, 2016; Chatterjee *et al.*, 2018; Naidoo *et al.*, 2018; Tordo *et al.*, 2018; Davidsson *et al.*, 2019). While a number of viral vectors have been described to retrogradely transduce neurons, these viruses may differ substantially in their tropism, or capacity and efficiency to drive transgene expression in different circuits and cell types (Wickersham *et al.*, 2007; Low *et al.*, 2013; Rothermel *et al.*, 2013). Such tools may be particularly useful for targeting classes of projection neurons for which cell type-specific gene promoters are not available or are otherwise unsuitable for viral transgene delivery, such as when the promoter sequence is too lengthy for viral packaging. The potential to use retrogradely-transducing vectors to target specific pathways make them particularly attractive to use in species for which transgenic models are not yet widely available, such as rats and non-human primates. In particular, there is an increasing trend towards the use of viral vectors to drive transgene expression in the NHP brain, both for basic neuroscientific and therapeutic research applications (Masamizu *et al.*, 2011; Gerits & Vanduffel, 2013; San Sebastian *et al.*, 2013; Porras *et al.*, 2014; Galvan *et al.*, 2018; Naidoo *et al.*, 2018). The neuroanatomical and functional similarities between NHP and human brains render these animal models particularly important for translationally-guided studies (Phillips *et al.*, 2014; Roelfsema & Treue, 2014), including pre-clinical evaluations of gene therapies (Mueller & Flotte, 2008).

Recently, a designer vector variant of recombinant adeno-associated virus serotype 2 was described (rAAV2-retro) with highly potent and selective retrograde transduction properties in the rodent brain (Tervo *et al.*, 2016). This vector was developed using an in vivo directed-evolution approach to screen and isolate rAAV variants that were efficiently trafficked from long-range projections to their parent soma. rAAV2-retro has emerged as a prominent retrograde vector for rodent neuroscientific studies, and may also provide a particularly useful tool for selective transduction of projection cell types in NHP brain, as alternative approaches for cell type-specific transgene delivery are highly limited in these model species (Galvan *et al.*, 2018). Interestingly, assessment of transgene labeling patterns following rAAV2-retro injections in mouse brain revealed that certain neuronal pathways were refractory to retrograde labeling (Tervo *et al.*, 2016). Whether such tropisms among retrograde vectors vary in a mammalian species-dependent manner is an important question that has not been systematically investigated.

With the long term goal of using rAAV2-retro as a tool to study specific neuronal pathways in NHPs, we have conducted light and electron microscopy observations of transgene labeling patterns following intra-striatal injections of the rAAV2-retro vector, encoding an opsin-conjugated green fluorescent protein (GFP) in rhesus macaques. We chose an opsin-encoding vector for these analyses due to the increasing use of optogenetic tools in NHP studies, and in recognition of the fact that viral expression patterns may vary by genetic payload (Rothermel *et al.*, 2013). The striatum was chosen as an injection target due to its well-defined input/output patterns, including both reciprocal and non-reciprocal long-range projections, as well as the importance of this region in a wide number of neurological and

neuropsychiatric diseases (Haber, 2003; Kreitzer & Malenka, 2008). Similar injections were done in parallel in rats, another genetically relatively non-tractable species, to evaluate the species specificity of the transduction patterns. EM ultrastructural observations were conducted in a subset of labeled basal ganglia regions in both species to identify putative sources of anterograde labeling evident in these structures, providing the first ultrastructural examination of neuronal elements labeled by rAAV2-retro. Overall, our results demonstrate that certain neural pathways may be refractory to transduction by retrograde vectors in a species-specific manner, highlighting the need for caution when determining the suitability of a retrograde vector for NHP studies based solely on rodent data. Our findings also indicate substantial anterograde transport of a transgene following rAAV2-retro-mediated retrograde transduction, providing evidence for a possible use of this method for connectome studies in rodents and primates.

Materials and Methods.

Subjects:

Three male Sprague-Dawley rats (Charles River, 300–350g), and 2 male rhesus macaques (*Maccaca Mulatta*; from the Yerkes Primate Center colony, 5 years old at time of surgery) were used in this study. All procedures were approved by the Animal Care and Use Committee of Emory University, and performed in accordance with the Guide for the Care and Use of Laboratory Animals (NRC, 2010) and the U.S. Public Health Service Policy on the Humane Care and Use of Laboratory Animals (revised 2015).

Viral Reagent:

For all described experiments, the rAAV2-retro vector was used (Tervo *et al.*, 2016), encoding the inhibitory opsin Jaws (Chuong *et al.*, 2014) conjugated to a GFP tag, under the human synapsin (hSyn) promoter (rAAV2-retro-hSyn-Jaws-KGC-GFP-ER2). Here, KGC and ER2 refer to trafficking sequences for the Kir2.1 potassium channel. Virus was obtained from Addgene (Cat. No. 65014-AAVrg; lot v32356) and used at a titer of 1.3×10^{13}.

Stereotactic Surgery (Rats):

Rats underwent a single surgery for intracranial injection of virus solution in the dorsomedial striatum, using sterile technique. Subjects were initially briefly sedated in an isoflurane induction chamber (4–5% isoflurane), and then placed in a stereotactic frame with nosecone adapter (Kopf, Tujunga, CA) (1.5–3% isoflurane for maintenance). Meloxicam (1–2mg/kg; s.c) was used as a surgical analgesic to reduce pain, administered once immediately prior to surgery and once daily for two days post-surgery. The surgical site was shaved and pre-treated with repeated ethanol and betadine swabs, followed by scalp incision and skull cleaning to visualize skull sutures. Ocular ointment was applied to prevent eye dryness during anesthesia. A rat stereotactic atlas (Paxinos & Watson, 2006) was used to define burr hole and subsequent injection coordinates, as follows (with reference to bregma and cortical surface): 0.4mm anterior, 3.4mm lateral, and 4.2mm ventral. In all cases, a total volume of 0.5µl was injected, at a rate of 0.1µl/min with an additional 5min post-injection diffusion period prior to needle withdrawal. Injections were administered using a Hamilton microsyringe (Reno, NE) coupled to an automated injector pump system (Stoelting, Wood

Dale, Il). Following injections, the skin was sutured and rats were recovered from anesthesia before returning to their home cage.

Stereotactic Surgery (Monkeys):

Monkeys underwent a surgery for intracranial injection of virus solution in the sensorimotor putamen, using sterile technique. Subjects were initially sedated with either ketamine (10mg/kg) or telazol (3–5mg/kg), intubated for isoflurane anesthesia (1–3%; intratracheal), and placed in a stereotactic frame. A craniotomy was performed, and the dura pierced using a 23g needle. A rhesus macaque stereotactic atlas (Paxinos *et al.*, 1999) was used to define the craniotomy and subsequent putamen injection coordinates, as follows: 14.7mm anterior to the interaural line, 14mm lateral to the midline, 20mm ventral from the cortical surface. In both monkeys, a total volume of 1.0μl of viral vector solution was unilaterally injected, at a rate of 0.2μl/min using the same injector pump system as described above for rat surgeries), allowing an additional 5min post-injection diffusion period prior to needle withdrawal. Following injections, the skin was sutured, and monkeys were recovered from anesthesia before being returned to their home cage. Post-operatively, animals were treated with buprenorphine (0.03mg/kg) and banamine (1mg/kg, both drugs being delivered every 6 hours for 3 days) to treat pain, and rocephin (25mg/kg for 7 days) to prevent infection.

Perfusion and Tissue Preparation:

All animals (rats and monkeys) were perfused approximately one month following surgery. At euthanasia, monkeys were deeply anesthetized with pentobarbital (100mg/kg; i.v.), while rats received an overdose of ketamine (50mg/kg) and xylazine (15–20mg/kg) delivered as a cocktail (i.p.). The animals were then transcardially perfused with an oxygenated Ringer's solution followed by a fixative made up of 4% paraformaldehyde and 0.1% glutaraldehyde. Brains were then taken out from the skull, post-fixed for 24 hours in 4% paraformaldehyde and cut in 60μm-thick sections with a vibrating microtome. Nissl staining was used to verify accuracy of injection tract placements.

Light Microscopy/ Immunohistochemistry:

Every fourth tissue section (rat and monkey) was labeled for GFP using previously described immunohistochemical procedures (Galvan *et al.*, 2016a; Galvan *et al.*, 2019; Albaugh *et al.*, 2020). Sections were first treated with 1% sodium borohydride (to retrieve antigens) and rinsed in phosphate-buffered saline (PBS; 0.01M, pH 7.4). Non-specific antibody binding sites were then blocked with 1% normal goat serum (NGS), 1% bovine serum albumin (BSA), and 0.3% Triton X-100 in PBS. Sections were then incubated for 24hr in a primary antibody solution containing the same blocking agents as well as an anti-GFP polyclonal antibody raised in rabbit (1:5000; Invitrogen, Waltham, MA, Cat No. A-11122; Lot 2083201; RRID AB_221569). This antibody results in highly specific labeling of GFP-positive cellular elements at both the light and electron microscopic levels, as previously described (Galvan *et al.*, 2016a). A subset of additional sections containing the substantia nigra were co-incubated with the GFP antibody and an anti-tyrosine hydroxylase (TH) monoclonal antibody raised in mouse (1:1000; Millipore, Burlington, MA, Cat No. MAB318; RRID AB_2201528) as described in prior publications from our group (Galvan *et al.*, 2010; Swain *et al.*, 2020).

For sections incubated with the anti-GFP antibody alone, primary antibody binding sites were revealed using the avidin-biotin complex (ABC) method (Hsu *et al.*, 1981). Sections were treated with a biotinylated goat anti-rabbit secondary antibody (1:200; Vector Laboratories, Burlingame, CA, Cat No. BA-100, RRID AB_2313606) for 60min, then exposed to an ABC solution (1:200; Vector Laboratories) including 1% BSA and 0.3% Triton X-100, for 90min, followed by rinses in PBS and then TRIS buffering solution (0.05M, pH 7.6). Next, sections were incubated in a TRIS buffer solution containing 0.025% 3,3'-diaminobenzidine tetrahydrochloride (DAB; Sigma, St. Louis, MO), 10mM Imidazole and 0.05% hydrogen peroxide for 10min, immediately followed by repeated PBS rinses to stop the peroxidase reaction. The incubation time for the DAB reaction was fixed to enable valid comparisons across subjects and species. All incubations were done at room temperature (RT). Sections were then mounted, cover slipped, and scanned (20x maximal magnification) with an Aperio Scanscope CS system (Leica, Wetzlar, Germany).

For sections co-incubated with anti-GFP and anti-TH primary antibodies, binding sites were revealed using two fluorophore-conjugated secondary antibodies, both raised in donkey: anti-rabbit FITC (1:100; Jackson, West Grove, PA, Cat No. 711-095-152, RRID AB_2315776) and anti-mouse rhodamine Red-X (1:100; Jackson, Cat No. 715-295-150, RRID AB_2340831). Sections were incubated for 60min (RT), rinsed in PBS, mounted with Vectashield (Vector Laboratories) and cover slipped. Slides were imaged using a confocal microscope (Leica DM5500B) equipped with a CCD camera (Orca R2; Hamamatsu).

Electron Microscopy/ Immunohistochemistry:

Based on the patterns of GFP labeling observed by light microscopy, a subset of tissue sections containing basal ganglia regions were chosen for electron microscopic analysis. Specifically, one block was prepared for EM analysis from each subject from the following regions (laterality defined relative to injected hemisphere): ipsilateral external globus pallidus (rat and monkey), ipsilateral subthalamic nucleus (rat and monkey), contralateral dorsal striatum (rat), and ipsilateral putamen (1–2mm ventral from targeted injection site, monkey). Additionally, a block containing the contralateral putamen was prepared from one of the two monkeys. Sections were prepared similarly to that described above for light microscopy, with some notable exceptions. Following sodium borohydride, the tissue was placed in a cryoprotectant solution, frozen at −80° C, thawed, and rinsed in phosphate-buffered saline (PBS; 0.01M, pH 7.4). Primary antibody incubation was performed at 4° C for 48hr. Triton-X-100 was also excluded from all solutions to prevent detergent-mediated loss of ultrastructural integrity.

Following secondary antibody labeling, sections were rinsed in PB (0.1M, pH 7.4) and then treated with 0.5% osmium tetroxide (OsO4) for 10min and returned to PB. Sections were then dehydrated with increasing concentrations of ethanol; 1% uranyl acetate was added to the 70% ethanol solution to increase EM contrast (10min in the dark). Sections were next placed in propylene oxide, followed by tissue embedding with an epoxy resin (Durcupan; Fluka, Buchs, Switzerland) for at least 12hr. Resin-embedded sections were then baked at 60 °C for at least 48hr until fully cured. Blocks containing regions of interest were obtained before being cut into ultrathin 60nm sections (Ultracut T2, Leica). These ultrathin sections

were mounted onto pioloform-coated grids and stained with lead citrate (5min) for added contrast. All incubations were done at RT. Grids were then examined with an electron microscope (EM; Jeol, Peabody, MA; Model 1011) coupled with a CCD camera (Gatan; Warrendale, PA; Model 785) which was controlled with Digital Micrograph Software (Gatan; Version 3.11.1). Sections were scanned and imaged in the EM at 40,000–60,000x magnification.

Two sets of images were acquired in the electron microscope: 1) To determine the relative proportion of pre- vs. postsynaptic elements immunolabeled in each section, all labeled elements that were randomly encountered in the tissue were imaged at 40,000x. These images were then analyzed to categorize immunostained structures as axon terminals or dendrites based on their distinct ultrastructural features (e.g., terminals defined by the presence of synaptic vesicles and apposition to dendrites) (Peters *et al.*, 1991). Thirty labeled elements were identified from these images for each subject/region. Labeled elements that could not be definitively categorized because of lack of clear ultrastructural features, or were neither axon terminals nor dendrites (e.g., myelinated axon or glia), were not quantified. 2) To determine the potential sources of GFP-labeled terminals, a second series of images of labeled axon terminals were acquired at 40,000–60,000x. For each immunoreactive terminal included in this dataset, their content in visible mitochondria and their cross-sectional diameter (as approximated in single section images) were recorded, in order to relate their ultrastructural features to terminals from known sources previously identified using anterograde tracing approaches (Shink *et al.*, 1996; Smith *et al.*, 1998). The presence or absence of GFP-positive cell bodies in our light microscopic analyses, as well as the location and type of synapses made (symmetric or asymmetric) were further considered in guiding interpretations of potential sources of labeled terminals in a given region.

Results.

Light Microscopic Observations

Rats: Rats received a single (unilateral), intra-striatal injection of an rAAV2-retro vector encoding the inhibitory opsin Jaws fused to the tag protein GFP. The location of the injection site was verified in Nissl stains (not shown). Examination of low-magnification images of GFP labeling near the injection tract in rat (and monkey) did not show obvious evidence of viral solution spread through damaged fiber tracts nor reflux along the injection tracts (Supp. Fig. 1), although the contributions of such unintended means of viral transduction cannot be entirely ruled out. The patterns of GFP labeling described below were consistent across the three rats used in this study.

In examining the resulting GFP-labeled tissue, we observed that the entire rostrocaudal axis of the dorsal striatum was bilaterally and diffusely labeled (Fig. 1A–C). Given that injections were unilateral, and that no labeled cell bodies were observed in the contralateral striatum, we reasoned that GFP labeling in the contralateral striatum likely arose from the axons of bilaterally-projecting intratelencephalic (IT) corticostriatal neurons (Shepherd, 2013). Consistently, deep-layer pyramidal cells were strongly labeled bilaterally in many cortical areas across the examined anteroposterior axis (Fig. 1D–E), with more labeled pyramidal cells in the hemisphere ipsilateral to injection (Supp. Fig. 2A). Strikingly, the perirhinal

cortex represented a “hotspot” of cortical GFP expression, with intense, discrete labeling observed bilaterally (Fig. 1E and Supp. Fig. 2B).

In the ipsilateral striatum, the dense neuropil labeling included labeled somata surrounding the injection site, although the high GFP labeling intensity in the area generally precluded definitive identification of all labeled striatal cells at the light microscopy level (Fig. 1A’). Retrograde labeling of striatal projection neurons may have occurred through their locally collateralizing axon terminals, and interneuron populations may have also been transduced. The strong intensity of neuropil labeling in the striatum distant from the injection site may have been due to the transduction of major striatal afferents, such as the corticostriatal and thalamostriatal pathways. Strong labelling in neuronal cell bodies was, indeed, observed ipsilaterally in several thalamic nuclei in all rats, including the intralaminar nuclei (central medial (CeM), centrolateral (CL) and parafascicular (PF) nuclei), as well as the ventral motor thalamic nuclei (Fig. 1F), reflecting the widespread origin of the robust thalamostriatal system (Berendse & Groenewegen, 1990; Smith *et al.*, 2004). The amygdalae (particularly the basolateral territory) were bilaterally labeled, (Fig. 1G and Supp. Fig. 2B), in agreement with the known projection patterns of the rat amygdalostriatal system (Russchen & Price, 1984). Additionally, we observed ipsilateral (but not contralateral) labeling in the external globus pallidus (GPe) and subthalamic nucleus (STN), including labeled cell bodies in both regions (Fig. 1B, C, H), likely reflecting the pallidostriatal and subthalamostriatal projections, respectively (Koshimizu *et al.*, 2013; Hegeman *et al.*, 2016). The substantia nigra (SN) contained labeled cell bodies in the compacta territory (SNc) and dense neuropil labeling in the pars reticulata (Fig. 1I). Although the labeled somata in STN and SNc were obscured by the intense neuropil staining (Figs. H’, I’), the GFP/TH immunofluorescence seen in the SNc (Fig. 3), as well as the EM observations collected from both areas confirmed the presence of GFP-positive cell bodies in these nuclei.

Monkeys: The two monkeys received a single (unilateral) injection of rAAV2-retro in the sensorimotor putamen (same virus and titer used in rat experiments). Nissl stains were used to verify the exact location of the injection sites (not shown). Results are reported for the hemisphere ipsilateral to the virus injection, unless otherwise noted. As in rats, dense GFP labeling was present throughout large portions of the striatum. The span of labeling, composed mostly of neuropil elements, exceeded 10mm rostrocaudally (mostly caudal to injection), and was observed in both the caudate nucleus and putamen (Fig. 2A–C). The neighboring GPe contained numerous GFP-positive neurons (indicating transduction in pallido-striatal neurons (Kita *et al.*, 1999)), in addition to dense neuropil labeling (Fig. 2A). The STN was also densely labeled, with many GFP-positive cell bodies, revealing the subthalamostriatal projection (Smith & Parent, 1986; Parent & Smith, 1987) (Fig. 2D). Cortical labeling was most prominent in frontal regions such as premotor and motor cortices, characterized by bands of GFP-positive deep-layer pyramidal neurons (Flaherty & Graybiel, 1991; Yeterian & Pandya, 1998) (Fig. 2E). In general, very few labeled cortical neurons were observed in the hemisphere contralateral to injection (Supp. Fig. 2C). The SN contained diffuse fiber and terminal-like labeling, with a few scattered GFP-positive cell bodies in the SNc (Fig. 2F). Finally, many GFP-positive neurons were found in the basolateral and basomedial nuclei of amygdala consistent with the known sources of the

amygdalostriatal system in primates (Russchen *et al.*, 1985; Smith & Parent, 1986) (Fig. 2G). However, in contrast to the observations made in rats, no GFP-positive cells or neuropil labeling were observed in the intralaminar thalamus, including the centromedian-parafascicular (CM-PF) complex (Fig. 2H), the main source of the thalamostriatal projection to both the caudate nucleus and putamen in monkeys (Galvan & Smith, 2011).

Another significant difference in the distribution of GFP labeling between rats and monkeys relates to the extent of anterograde labeling in the contralateral striatum. While the neuropil of the entire contralateral striatum was heavily stained in rats (Fig. 1C), GFP-positive fibers were confined to a few clusters in the dorsolateral part of the post-commissural putamen in one of the monkeys (Supp. Fig. 2D) and absent for the other, despite strong ipsilateral striatal GFP staining in both animals. Assuming that this contralateral striatal labeling originates predominantly from contralateral IT corticostriatal neurons, the species difference can be explained by the heavy *versus* sparse expression of GFP-positive cells in the contralateral cortices in rats and monkeys, respectively (see Supp. Fig. 2C for representative examples of labeling in the contralateral motor cortex of monkey). An ultrastructural analysis of the morphology and synaptic connectivity of the GFP-labeled terminals in the contralateral putamen was performed to confirm the cortical origin of these terminals (see Electron Microscopic Observations).

A final point of observation from this data relates to the claustrum, which was prominently labeled in the ipsilateral hemisphere of the monkey, including numerous labeled cells (Supp. Fig. 3A–B). Although the claustrum proper was not similarly labeled in rats, we did note labeled cells within the dorsal endopiriform nucleus (Supp. Fig. 3C–D), which may be anatomically and functionally complexed with the claustrum in rodents (Smith *et al.*, 2019).

Substantia Nigra Pars Compacta (SNc) GFP/ Tyrosine Hydroxylase (TH) Co-labeling: In the initial description of rAAV2-retro, it was noteworthy that the virus showed only sparse labeling of the nigrostriatal pathway following intra-striatal viral injections in mice (Tervo *et al.*, 2016). In our rat experiments, we observed some GFP-positive cell bodies in the pars compacta territory (SNc) and profuse axonal and terminal-like labeling in the pars reticulata (SNr) (Fig. 1I). In the monkeys, however, our light microscopy observations revealed only sparse cell body staining in the SNc and a rich plexus of labeled neuropil in the lateral tier of the SNr (Fig. 2F). To verify if the GFP-positive cells observed in the rat SNc were dopaminergic nigrostriatal neurons, we double immunostained rat and monkey nigral sections for GFP and TH. A modest overlap between GFP and TH immunoreactivity was found in rat SNc neurons (Fig. 3A), demonstrating partial labeling of the nigrostriatal pathway in this species, and consistent with earlier data reported for mice (Tervo *et al.*, 2016). Some GFP-immunoreactive cells displayed weak or no significant TH labeling, suggesting that these were non-dopaminergic (e.g., glutamatergic) SNc neurons (Yamaguchi *et al.*, 2013). It may also be possible that AAV-mediated transduction could downregulate expression of TH (Albert *et al.*, 2019). In contrast to rat, and as anticipated based on the GFP immunoperoxidase staining, sparse GFP-positive fibers were present in the monkey SNc, but double GFP+/TH+ cell bodies could not be found (Fig. 3B).

Electron Microscopic (EM) Observations: The functional implications of transgene expression in a given brain region may largely depend upon the subcellular elements expressing the transgene (e.g., axonal vs. dendritic expression), as well as the sources and connectivity of those elements. The basal ganglia network in both rodents and primates is characterized by a large degree of regional interconnectivity, presenting a considerable challenge in identifying the source(s) of axonal and terminal labeling by retrograde tracers and viruses (including rAAV2-retro) injected into basal ganglia structures. Although light microscopy observations are, in most cases, sufficient to identify neuronal somata and proximal dendrites, the characterization of neuropil elements remains tentative because these can include a mixture of pre- and postsynaptic components (dendritic, axonal and terminal profiles, respectively). Electron microscopy is a reliable tool for ultrastructural identification of immunopositive structures. In the various basal ganglia nuclei, the ultrastructural features (e.g., terminal size, relative abundance of mitochondria, postsynaptic targets, symmetric vs asymmetric synaptic specialization) of various populations of axon terminals have been well characterized, providing a solid foundation for identifying the potential source(s) of GFP-labeled terminals identified in the present study (Dubé *et al.*, 1988; Shink *et al.*, 1996; Smith *et al.*, 1998). Thus, we employed electron microscopy to characterize the putative sources of labeled presynaptic terminals in a subset of GFP-containing basal ganglia nuclei. For these analyses, we specifically focused on regions in which ultrastructural features were likely to provide the most conclusive evidence regarding the origins of labeled elements.

Rat Experiments

General Neuropil Labeling: To discern the contributions of pre- and postsynaptic labeling in the GFP-labeled neuropil observed in the rat basal ganglia, we first quantified the relative proportions of labeled dendrites and axon terminals that were randomly encountered in EM sections acquired from the GPe and STN ipsilateral to virus injection, and the contralateral dorsal striatum. Representative EM images from these regions are included in Fig. 4A–D. Of encountered elements that could be identified as either axon terminals or dendrites, 41% were axonal terminals in the GPe, while only 9% were identified as such in the STN (GPe: 37/90; STN: 8/90 counted elements; n= 3 rats for both regions). These findings suggest that the labeled neuropil in the GPe includes a mixture of both pre- and postsynaptic elements, while the STN is, for the most part, composed of postsynaptic elements. On the other hand, the contralateral striatum contained only labeled axon terminals (90/90 counted elements, n= 3 rats), consistent with the lack of labeled cell bodies observed in this region by light microscopy. For the two regions evaluated that exhibited significant presynaptic labeling (contralateral striatum and ipsilateral GPe), we next characterized the ultrastructural features of labeled axon terminals.

Terminal Labeling in Contralateral Striatum: The neuropil of the whole contralateral striatum was heavily GFP-immunostained after unilateral striatal rAAV2-retro injection (Fig. 1C). In light of the known striatal connectivity, retrogradely transduced IT corticostriatal neurons in contralateral cortices represent the most likely source of this dense innervation (Reiner *et al.*, 2010). Consistent with this hypothesis, our electron microscopy analysis of 90 GFP-immunoreactive terminals revealed that they all displayed the ultrastructural features of

corticostriatal boutons (less than 1.5μm in diameter, 0–2 mitochondria) (Fig. 4E) (Lei *et al.*, 2004) and formed asymmetric axo-spinous asymmetric synapses (Fig. 4A).

Terminal Labeling in Ipsilateral GPe: The ipsilateral rat GPe contained a large number of GFP-immunoreactive neuronal cell bodies within a rich meshwork of labeled terminal-like profiles. Based on the pattern of distribution of retrogradely transduced neurons with known projections to the GPe, the most likely sources of these terminals could be axon collaterals of GFP-containing glutamatergic subthalamostriatal neurons or GABAergic striatopallidal projections (Fig. 1A, H). Electron microscopic analysis of 44 GFP-positive terminals revealed that they had a cross sectional diameter not larger than 2.0μm, and more than half (24/44 terminals) had fewer than three mitochondria (Fig. 4E). When observed, synapses formed by these terminals were asymmetric and axo-dendritic. These ultrastructural features are reminiscent of those described for subthalamopallidal terminals, but different from striatopallidal boutons, which invariably form symmetric axo-dendritic synapses (Smith *et al.*, 1998).

Monkey Experiments

General Neuropil Labeling: As described above for rats, we quantified the relative proportions of labeled dendrites and axon terminals that were randomly encountered in EM sections obtained from a subset of labeled basal ganglia regions. In monkey, we examined the putamen both ipsi- and contralateral to virus injection (ipsilateral side taken 1–2mm away from injection site), as well as the GPe and STN. Representative EM images from these regions are shown in Fig. 5A–D. In the ipsilateral putamen, labeled elements were predominantly axonal. Of the encountered elements that could be identified as either axon terminals or dendrites, 97% were categorized as axon terminals (58/60 counted elements, n= 2 monkeys). Similarly, in the contralateral putamen, 100% of encountered labeled elements were axon terminals (30/30 counted elements, n= 1 monkey). In contrast, in the GPe and STN, labeled elements were mostly dendritic. Of the total number of labeled profiles that could be identified in these two nuclei, 13% and 2% were axon terminals in the GPe and STN, respectively (GPe: 8/60 counted elements; STN: 1/60 counted elements; n= 2 monkeys for each region). The reduced prevalence of labeled STN-like terminals in the monkey GPe compared to rats could be due to a smaller relative proportion and a more restricted localization of retrogradely-labeled neurons in the monkey than in the rat STN (compare Fig. 1H and 2D). For the ipsi- and contralateral putamen, the two regions evaluated that exhibited significant presynaptic labeling, we next characterized the ultrastructural features of labeled axon terminals.

Terminal Labeling in Ipsilateral Putamen away from Injection Site: As described above, the GFP immunostaining in the neuropil of the ipsilateral putamen extended as far as 10mm away from the injection site (generally caudally) (Fig. 2A, C). The sources of this extensive labeling could be axon terminals from retrogradely transduced GABAergic projection neurons and interneurons within the striatum or extrinsic glutamatergic afferents from GFP-labeled cells in cortex and STN. Analysis of 35 randomly encountered labeled terminals revealed that they all displayed ultrastructural features (less than 2.0μm in diameter, generally fewer than 3 mitochondria, asymmetric axo-spinous synapses) (Fig. 5A, E) typical

of glutamatergic afferents from cortex and thalamus (Dubé *et al.*, 1988; Sadikot *et al.*, 1992), and possibly also STN (Koshimizu *et al.*, 2013). Because the thalamus was devoid of retrogradely transduced neurons in monkeys, the cortex and STN are considered as the main sources of this striatal innervation. These EM observations also suggest that the extensive GFP immunostaining within the injected striatum does not represent the extent of virus spread within the injected target, but rather reflects the massive extrinsic glutamatergic innervation of the striatum by the cortex and STN. The absence of GFP-labeled terminals forming symmetric synapses suggests that transduced terminals from striatal interneurons or local collaterals of striatal projection neurons were not present in the analyzed material, which may be due to the distant site (1–2mm) from which these blocks were taken relative to the injection target. Further studies would be needed to evaluate the contribution of these local projections to the labeled striatal neuropil, particularly in regions more proximal to the injection site.

Terminal Labeling in the Contralateral Putamen: As shown in Supp. Fig. 2D, the contralateral putamen contained clusters of GFP-immunoreactive terminal profiles (in one of the two monkeys studied). Electron microscopic analysis of 15 randomly encountered terminals indicated that they displayed the ultrastructural features of cortical boutons revealed in previous tract-tracing monkey studies (Smith *et al.*, 1994) (i.e. less than 2.0μm in diameter, generally fewer than 3 mitochondria, asymmetric axo-spinous synapses) (Fig. 5B, E). These observations suggest that the sources of this contralateral striatal innervation are the retrogradely transduced IT corticostriatal neurons in the contralateral motor cortices (Supp. Fig. 2C).

Discussion.

In this study, we have evaluated the suitability of the recently-described rAAV2-retro vector for labeling striatal inputs in rats and NHPs. As reported previously in mice (Tervo *et al.*, 2016) and macaques (Cushnie *et al.*, 2020; Weiss *et al.*, 2020), we found that intra-striatal injections of rAAV2-retro resulted in abundant labeling in numerous cortical and subcortical regions (summarized in Fig. 6). Within the basal ganglia, retrograde transport was observed in the GPe and STN, regions known to project to the striatum, in both species. In contrast, the nigrostriatal projection was modestly labeled in rats, but not in monkeys. Additionally, the thalamostriatal pathway, a massive source of glutamatergic inputs to the striatum (Sadikot *et al.*, 1992; Smith *et al.*, 2004), was strongly labeled in rats after rAAV2-retro intra-striatal injections, but not in monkeys, indicating important species differences in the tropism of this virus. For the first time, we conducted ultrastructural analyses of the basal ganglia nuclei labeled after striatal injections of rAAV2-retro to help characterize the sources of GFP-labeled terminals in these nuclei. In most regions, the labeling was found in both postsynaptic dendrites and presynaptic axonal terminals; the latter likely derived from anterograde transgene transport in neurons that project to the injection site, as well as from axon collaterals of these neurons that project to other sites. Using knowledge from previous anterograde tracing studies about the ultrastructural features and synaptic architecture of specific subsets of axon terminals to basal ganglia regions (Shink *et al.*, 1996; Smith *et al.*,

1998), we could better understand the organization of functional networks labeled with rAAV2-retro in NHPs.

Recently, a study reported viral transduction patterns following intra-striatal infusions of rAAV2-retro in rhesus macaques (Weiss *et al.*, 2020) (see also (Cushnie *et al.*, 2020)). The transgene (GFP) labeling patterns described by Weiss et al. are similar to those reported here, which is remarkable given some important differences in viral injection parameters. Weiss et al. performed multiple injections in each animal (2 sites in putamen, 1 in caudate head) to deliver a total volume of 230μl of viral vector solution in the striatum. In our experiments, despite the fact that each monkey received a single putamen injection of 1μl of rAAV2-retro, we observed similar transduction patterns (although we cannot directly compare the actual areas covered by the injections in each case). This is notable, as large injection volumes are time consuming, and may not be feasible when performing viral infusions using electrophysiological guidance of injection targeting in awake, behaving animals (Kliem & Wichmann, 2004; Galvan *et al.*, 2018). Small injection volumes are also preferable for reducing spread of viral solution to neighboring regions outside of the intended injection target, which is particularly challenging to evaluate with retrograde vectors (see below). Indeed, certain anatomical regions in which Weiss et al. reported rAAV2-retro-mediated neuronal transduction, such as the reticular nucleus of the thalamus and internal globus pallidus, have no known projections to striatum in NHP, suggesting the possibility of viral solution spread outside of the striatum (as also acknowledged by the authors). Other important differences between Weiss et al. 2020 and the present study is that the rAAV2-retro viral titer used by our group was tenfold higher than that used by Weiss and colleagues, and that the promoter we used (hSyn) may have greater transduction efficiency for neurons in NHP brain compared to the human cytomegalovirus (CMV) promoter used by Weiss et al. (at least in neocortex) (Gerits *et al.*, 2015). Additional work is needed to determine the optimal promoter choices for rAAV2-retro-based studies in NHPs, which may be circuit-specific. Despite the numerous parametric differences in the viral injections between these two studies, Weiss et al. also found a lack of transgene labeling of the CM-PF thalamus, further suggesting that in NHPs this pathway is refractory to labeling by the rAAV2-retro vector *per se*. However, Weiss and colleagues did describe thalamic labeling in other regions, including the mediodorsal thalamus; thus, that not all striatal-projecting thalamic nuclei may be refractory to retrograde transduction by this vector.

Species Differences in Transgene Expression:

Variation in transgene expression patterns could be mediated by a combination of factors that influence virus tropism, including the vector capsid, the titer of the virus solution, the gene promoter used and the injection method. In our study, we used the same viral construct, at an identical concentration, in both rat and NHP, as well as a gene promoter (hSyn) known to restrict transgene expression to neurons in rat (Kugler *et al.*, 2003) and NHPs (Diester *et al.*, 2011). Regardless of these similarities, we observed a lack of transgene expression in the NHP intralaminar thalamus. We have previously observed robust virally-mediated neuronal transgene expression in CM-PF thalamus after a local injection of AAV5-hSyn-GFP (Galvan *et al.*, 2016b), arguing that the presently observed species differences in rAAV2-retro tropism are likely due to the vector per se, rather than the gene promoter. This result, along

with the poor transduction of the nigrostriatal pathway, suggest that rAAV2-retro should be tested for appropriate transduction of specific pathways, particularly in NHPs. Interestingly, a recent study suggests that CAV-2 may be a suitable alternative retrograde viral vector for targeting the thalamostriatal system in NHPs (di Caudo *et al.*, 2020).

Technical Challenges with Retrograde Vectors.

A major technical challenge associated with the use of rAAV2-retro and similar retrogradely-transducing vectors is to determine the extent of viral spread at the site(s) of injection. Such knowledge may be critically important for both verifying injection accuracy and interpreting the source(s) of transduced long-distance projections (as they anatomically relate to the injected territory). Besides being captured by the terminals, there is evidence that rAAV2-retro viral particles are also captured by cell bodies at the injection site (Tervo *et al.*, 2016). Thus, in theory, the spread of the virus solution could be evaluated by assessing the number or proportion of transduced somata surrounding the injection site. This approach, however, does not inform about the sources and extent of locally-transduced terminal fields. The interpretation of these observations is further complicated if retrogradely-transduced labeled neurons provide diffuse inputs to the injected territory. Our data indicate that the use of EM combined with literature knowledge about the ultrastructural features of specific afferent terminals to the injected target can help address this issue. For instance, our EM analysis of the extensive GFP-immunostained neuropil 1–2mm away from the injection site in the ipsilateral monkey putamen indicated that the bulk of this immunoreactivity comprised almost exclusively presynaptic terminal profiles forming asymmetric synapses, suggesting that the spread of the injected virus may have been less than 1mm, and that extrinsic glutamatergic inputs (from cortex or STN) innervate widespread striatal regions beyond the confines of the injected target region. Due to the extensive and varied sources of labeled terminals anticipated to be present in the ipsilateral rat striatum, we did not conduct a similar ultrastructural analysis in this species. Such an examination may be an important focus for future studies using rAAV2-retro or other retrograde vectors.

Future Directions.

Our primary motivation for this study was to evaluate the suitability of rAAV2-retro for transducing long-range inputs to the NHP striatum, including parallel rodent experiments as a source of comparison. Overall, we were encouraged to find that most expected major projections to the striatum were transduced by this vector in NHPs. However, as we have noted, the labeling of thalamostriatal projection neurons in rat, but not NHP, is a major discrepancy that highlights the need for pilot testing of viral approaches in NHPs when possible, and caution in generalizing observations of viral tropism from one animal species to others. The lack of SNc dopamine cell labeling in NHPs should also be highlighted in this context, given recent and ongoing gene therapy efforts to transduce the nigrostriatal pathway with retrograde viral vectors in Parkinson's Disease (Marks *et al.*, 2010; Smith *et al.*, 2012). In this regard, a pseudotyped lentiviral vector with retrograde transduction properties has been described to have the capability to target the nigrostriatal pathway in primates (Tanabe *et al.*, 2017). Additional, recently described retrograde AAVs have also been shown to label the thalamostriatal system in rodents (Tordo *et al.*, 2018; Davidsson *et al.*, 2019), and further

testing of these variants in NHP may be warranted. Despite these potential caveats, our results encourage further use of rAAV2-retro for mapping and functionally interrogating neural circuits in NHPs.

We are particularly enthusiastic about the possibility of employing rAAV2-retro and other retrograde vectors in NHP studies in the context of intersectional genetic strategies to isolate and manipulate neuronal cell types based on projection patterns, and avoid transgene expression in brain regions that receive axonal collaterals of neurons that project to the injected target. The use of dual-viral conditional expression approaches, in which a recombinase enzyme packaged by rAAV2-retro is injected within a terminal field, alongside a recombination-dependent genetic label/actuator at the location of the targeted cell bodies, may be particularly important in isolating specific neuronal pathways.

Supplementary Material

Refer to Web version on PubMed Central for supplementary material.

Acknowledgements:

The authors thank X. Hu, J.F. Paré and S. Jenkins for technical assistance. This work was supported by NIH grants 1R01NS100908 (awarded to A.G), P50-NS098685 (Udall Center grant) and P51-OD011132 (Yerkes Center base grant), as well as a postdoctoral fellowship from the Parkinson's Foundation (PF-FBS-1928; awarded to D.L.A). None of the authors have any conflicts of interest to report.

Data Availability Statement: The data that support the findings of this study are available from the corresponding author upon reasonable request.

References.

Albaugh DL, Huang C, Ye S, Paré JF & Smith Y (2020) Glutamatergic inputs to GABAergic interneurons in the motor thalamus of control and parkinsonian monkeys. Eur. J. Neurosci

Albert K, Voutilainen MH, Domanskyi A, Piepponen TP, Ahola S, Tuominen RK, Richie C, Harvey BK & Airavaara M (2019) Downregulation of tyrosine hydroxylase phenotype after AAV injection above substantia nigra: Caution in experimental models of Parkinson's disease. J. Neurosci. Res, 97, 346–361. [PubMed: 30548446]

Berendse HW & Groenewegen HJ (1990) Organization of the thalamostriatal projections in the rat, with special emphasis on the ventral striatum. J. Comp. Neurol, 299, 187–228. [PubMed: 2172326]

Chatterjee S, Sullivan HA, MacLennan BJ, Xu R, Hou Y, Lavin TK, Lea NE, Michalski JE, Babcock KR, Dietrich S, Matthews GA, Beyeler A, Calhoon GG, Glober G, Whitesell JD, Yao S, Cetin A, Harris JA, Zeng H, Tye KM, Reid RC & Wickersham IR (2018) Nontoxic, double-deletion-mutant rabies viral vectors for retrograde targeting of projection neurons. Nat. Neurosci, 21, 638–646. [PubMed: 29507411]

Chuong AS, Miri ML, Busskamp V, Matthews GA, Acker LC, Sorensen AT, Young A, Klapoetke NC, Henninger MA, Kodandaramaiah SB, Ogawa M, Ramanlal SB, Bandler RC, Allen BD, Forest CR, Chow BY, Han X, Lin Y, Tye KM, Roska B, Cardin JA & Boyden ES (2014) Noninvasive optical inhibition with a red-shifted microbial rhodopsin. Nat. Neurosci, 17, 1123–1129. [PubMed: 24997763]

Cushnie AK, El-Nahal HG, Bohlen MO, May PJ, Basso MA, Grimaldi P, Wang MZ, de Velasco EMF, Sommer MA & Heilbronner SR (2020) Using rAAV2-retro in rhesus macaques: Promise and caveats for circuit manipulation. J. Neurosci. Methods, 108859. [PubMed: 32668316]

Davidsson M, Wang G, Aldrin-Kirk P, Cardoso T, Nolbrant S, Hartnor M, Mudannayake J, Parmar M & Bjorklund T (2019) A systematic capsid evolution approach performed in vivo for the design of AAV vectors with tailored properties and tropism. Proc. Natl. Acad. Sci. U.S.A

di Caudo C, Martinez-Valbuena I, Mundinano IC, Gennetier A, Hernandez M, Carmona-Abellan M, Marcilla Garcia I, Kremer EJ & Luquin R (2020) CAV-2-Mediated GFP and LRRK2(G2019S) Expression in the Macaca fascicularis Brain. Front. Mol. Neurosci, 13, 49. [PubMed: 32269512]

Diester I, Kaufman MT, Mogri M, Pashaie R, Goo W, Yizhar O, Ramakrishnan C, Deisseroth K & Shenoy KV (2011) An optogenetic toolbox designed for primates. Nat. Neurosci, 14, 387–397. [PubMed: 21278729]

Dubé L, Smith AD & Bolam JP (1988) Identification of synaptic terminals of thalamic or cortical origin in contact with distinct medium-size spiny neurons in the rat neostriatum. J. Comp. Neurol, 267, 455–471. [PubMed: 3346370]

Flaherty A & Graybiel A (1991) Corticostriatal transformations in the primate somatosensory system. Projections from physiologically mapped body-part representations. J. Neurophysiol, 66, 1249–1263. [PubMed: 1722244]

Galvan A, Caiola MJ & Albaugh DL (2018) Advances in optogenetic and chemogenetic methods to study brain circuits in non-human primates. J. Neural Transm. (Vienna), 125, 547–563. [PubMed: 28238201]

Galvan A, Hu X, Smith Y & Wichmann T (2010) Localization and function of GABA transporters in the globus pallidus of parkinsonian monkeys. Exp. Neurol, 223, 505–515. [PubMed: 20138865]

Galvan A, Hu X, Smith Y & Wichmann T (2016a) Effects of optogenetic activation of corticothalamic terminals in the motor thalamus of awake monkeys. J. Neurosci, 36, 3519–3530. [PubMed: 27013680]

Galvan A, Hu X, Smith Y & Wichmann T (2016b) Effects of optogenetic activation of thalamostriatal terminals in monkeys Society for Neuroscience, San Diego, CA Abstract No. 415.22.

Galvan A, Raper J, Hu X, Pare JF, Bonaventura J, Richie CT, Michaelides M, Mueller SAL, Roseboom PH, Oler JA, Kalin NH, Hall RA & Smith Y (2019) Ultrastructural localization of DREADDs in monkeys. Eur. J. Neurosci, 50, 2801–2813. [PubMed: 31063250]

Galvan A & Smith Y (2011) The primate thalamostriatal systems: Anatomical organization, functional roles and possible involvement in Parkinson's disease. Basal Ganglia, 1, 179–189. [PubMed: 22773963]

Gerits A, Vancraeyenest P, Vreysen S, Laramee ME, Michiels A, Gijsbers R, Van den Haute C, Moons L, Debyser Z, Baekelandt V, Arckens L & Vanduffel W (2015) Serotype-dependent transduction efficiencies of recombinant adeno-associated viral vectors in monkey neocortex. Neurophotonics, 2, 031209. [PubMed: 26839901]

Gerits A & Vanduffel W (2013) Optogenetics in primates: a shining future? Trends Genet, 29, 403–411. [PubMed: 23623742]

Haber SN (2003) The primate basal ganglia: parallel and integrative networks. J. Chem. Neuroanat, 26, 317–330. [PubMed: 14729134]

Hegeman DJ, Hong ES, Hernandez VM & Chan CS (2016) The external globus pallidus: progress and perspectives. Eur. J. Neurosci, 43, 1239–1265. [PubMed: 26841063]

Hollis II ER, Kadoya K, Hirsch M, Samulski RJ & Tuszynski MH (2008) Efficient Retrograde Neuronal Transduction Utilizing Self-complementary AAV1. Mol. Ther, 16, 296–301.

Hsu S-M, Raine L & Fanger H (1981) Use of avidin-biotin-peroxidase complex (ABC) in immunoperoxidase techniques: a comparison between ABC and unlabeled antibody (PAP) procedures. J. Histochem. Cytochem, 29, 577–580. [PubMed: 6166661]

Kato S, Kobayashi K, Inoue K, Kuramochi M, Okada T, Yaginuma H, Morimoto K, Shimada T, Takada M & Kobayashi K (2011) A lentiviral strategy for highly efficient retrograde gene transfer by pseudotyping with fusion envelope glycoprotein. Hum. Gene Ther, 22, 197–206. [PubMed: 20954846]

Kita H, Tokuno H & Nambu A (1999) Monkey globus pallidus external segment neurons projecting to the neostriatum. Neuroreport, 10, 1467–1472. [PubMed: 10380964]

Kliem MA & Wichmann T (2004) A method to record changes in local neuronal discharge in response to infusion of small drug quantities in awake monkeys. J. Neurosci. Methods, 138, 45–49. [PubMed: 15325110]

Koshimizu Y, Fujiyama F, Nakamura KC, Furuta T & Kaneko T (2013) Quantitative analysis of axon bouton distribution of subthalamic nucleus neurons in the rat by single neuron visualization with a viral vector. J. Comp. Neurol, 521, 2125–2146. [PubMed: 23595816]

Kreitzer AC & Malenka RC (2008) Striatal plasticity and basal ganglia circuit function. Neuron, 60, 543–554. [PubMed: 19038213]

Kugler S, Kilic E & Bahr M (2003) Human synapsin 1 gene promoter confers highly neuron-specific long-term transgene expression from an adenoviral vector in the adult rat brain depending on the transduced area. Gene Ther, 10, 337–347. [PubMed: 12595892]

Lei W, Jiao Y, Del Mar N & Reiner A (2004) Evidence for differential cortical input to direct pathway versus indirect pathway striatal projection neurons in rats. J. Neurosci, 24, 8289–8299. [PubMed: 15385612]

Low K, Aebischer P & Schneider BL (2013) Direct and retrograde transduction of nigral neurons with AAV6, 8, and 9 and intraneuronal persistence of viral particles. Hum. Gene Ther, 24, 613–629. [PubMed: 23600720]

Marks WJ, Bartus RT, Siffert J, Davis CS, Lozano A, Boulis N, Vitek J, Stacy M, Turner D, Verhagen L, Bakay R, Watts R, Guthrie B, Jankovic J, Simpson R, Tagliati M, Alterman R, Stern M, Baltuch G, Starr PA, Larson PS, Ostrem JL, Nutt J, Kieburtz K, Kordower JH & Olanow CW (2010) Gene delivery of AAV2-neurturin for Parkinson's disease: a double-blind, randomised, controlled trial. Lancet Neurol., 9, 1164–1172. [PubMed: 20970382]

Masamizu Y, Okada T, Kawasaki K, Ishibashi H, Yuasa S, Takeda S, Hasegawa I & Nakahara K (2011) Local and retrograde gene transfer into primate neuronal pathways via adeno-associated virus serotype 8 and 9. Neuroscience, 193, 249–258. [PubMed: 21782903]

Mueller C & Flotte TR (2008) Clinical gene therapy using recombinant adeno-associated virus vectors. Gene Ther., 15, 858–863. [PubMed: 18418415]

Naidoo J, Stanek LM, Ohno K, Trewman S, Samaranch L, Hadaczek P, O'Riordan C, Sullivan J, San Sebastian W, Bringas JR, Snieckus C, Mahmoodi A, Mahmoodi A, Forsayeth J, Bankiewicz KS & Shihabuddin LS (2018) Extensive Transduction and Enhanced Spread of a Modified AAV2 Capsid in the Non-human Primate CNS. Mol. Ther, 26, 2418–2430. [PubMed: 30057240]

Nassi JJ, Cepko CL, Born RT & Beier KT (2015) Neuroanatomy goes viral! Front. Neuroanat, 9, 80. [PubMed: 26190977]

NRC (2010) Guide for the care and use of laboratory animals. National Academies Press, Washington, D.C.

Parent A & Smith Y (1987) Organization of efferent projections of the subthalamic nucleus in the squirrel monkey as revealed by retrograde labeling methods. Brain Res., 436, 296–310. [PubMed: 3435830]

Paxinos G, Huang X-F & Toga AW (1999) The rhesus monkey brain in stereotaxic coordinates. Academic Press, San Diego, USA.

Paxinos G & Watson C (2006) The rat brain in stereotaxic coordinates. Elsevier.

Peters A, Palay S & Webster H (1991) The fine structure of the nervous system. Oxford University Press, New York.

Phillips KA, Bales KL, Capitanio JP, Conley A, Czoty PW, 't Hart BA, Hopkins WD, Hu SL, Miller LA & Nader MA (2014) Why primate models matter. Am. J. Primatol, 76, 801–827. [PubMed: 24723482]

Porras G, Dehay B & Bezard E (2014) Viral vectors in primate research: examples from Parkinson's disease research Viral Vector Approaches in Neurobiology and Brain Diseases. Springer, pp. 331–341.

Reiner A, Hart NM, Lei W & Deng Y (2010) Corticostriatal projection neurons - dichotomous types and dichotomous functions. Front. Neuroanat, 4, 142. [PubMed: 21088706]

Roelfsema PR & Treue S (2014) Basic neuroscience research with nonhuman primates: a small but indispensable component of biomedical research. Neuron, 82, 1200–1204. [PubMed: 24945764]

Rothermel M, Brunert D, Zabawa C, Diaz-Quesada M & Wachowiak M (2013) Transgene expression in target-defined neuron populations mediated by retrograde infection with adeno-associated viral vectors. J. Neurosci, 33, 15195–15206. [PubMed: 24048849]

Russchen F, Bakst I, Amaral DG & Price J (1985) The amygdalostriatal projections in the monkey. An anterograde tracing study. Brain Res., 329, 241–257. [PubMed: 3978445]

Russchen FT & Price JL (1984) Amygdalostriatal projections in the rat. Topographical organization and fiber morphology shown using the lectin PHA-L as an anterograde tracer. Neurosci. Lett, 47, 15–22. [PubMed: 6087218]

Sadikot A, Parent A, Smith Y & Bolam J (1992) Efferent connections of the centromedian and parafascicular thalamic nuclei in the squirrel monkey: a light and electron microscopic study of the thalamostriatal projection in relation to striatal heterogeneity. J. Comp. Neurol, 320, 228–242. [PubMed: 1619051]

San Sebastian W, Samaranch L, Heller G, Kells AP, Bringas J, Pivirotto P, Forsayeth J & Bankiewicz KS (2013) Adeno-associated virus type 6 is retrogradely transported in the non-human primate brain. Gene Ther., 20, 1178–1183. [PubMed: 24067867]

Shepherd GM (2013) Corticostriatal connectivity and its role in disease. Nat. Rev. Neurosci, 14, 278–291. [PubMed: 23511908]

Shink E, Bevan M, Bolam J & Smith Y (1996) The subthalamic nucleus and the external pallidum: two tightly interconnected structures that control the output of the basal ganglia in the monkey. Neuroscience, 73, 335–357. [PubMed: 8783253]

Smith JB, Alloway KD, Hof PR, Orman R, Reser DH, Watakabe A & Watson GDR (2019) The relationship between the claustrum and endopiriform nucleus: A perspective towards consensus on cross-species homology. J. Comp. Neurol, 527, 476–499. [PubMed: 30225888]

Smith Y, Bennett B, Bolam J, Parent A & Sadikot A (1994) Synaptic relationships between dopaminergic afferents and cortical or thalamic input in the sensorimotor territory of the striatum in monkey. J. Comp. Neurol, 344, 1–19. [PubMed: 7914894]

Smith Y, Bevan M, Shink E & Bolam JP (1998) Microcircuitry of the direct and indirect pathways of the basal ganglia. Neuroscience, 86, 353–387. [PubMed: 9881853]

Smith Y & Parent A (1986) Differential connections of caudate nucleus and putamen in the squirrel monkey (Saimiri sciureus). Neuroscience, 18, 347–371. [PubMed: 3736862]

Smith Y, Raju DV, Pare J-F & Sidibe M (2004) The thalamostriatal system: a highly specific network of the basal ganglia circuitry. Trends Neurosci., 27, 520–527. [PubMed: 15331233]

Smith Y, Wichmann T, Factor SA & DeLong MR (2012) Parkinson's disease therapeutics: new developments and challenges since the introduction of levodopa. Neuropsychopharmacology, 37, 213–246. [PubMed: 21956442]

Soudais C, Laplace-Builhe C, Kissa K & Kremer EJ (2001) Preferential transduction of neurons by canine adenovirus vectors and their efficient retrograde transport in vivo. FASEB J., 15, 2283–2285. [PubMed: 11511531]

Swain AJ, Galvan A, Wichmann T & Smith Y (2020) Structural plasticity of GABAergic and glutamatergic networks in the motor thalamus of parkinsonian monkeys. J. Comp. Neurol, 528, 1436–1456. [PubMed: 31808567]

Tanabe S, Inoue K. i., Tsuge H, Uezono S, Nagaya K, Fujiwara M, Kato S, Kobayashi K & Takada M (2017) The use of an optimized chimeric envelope glycoprotein enhances the efficiency of retrograde gene transfer of a pseudotyped lentiviral vector in the primate brain. Neurosci. Res, 120, 45–52. [PubMed: 28257798]

Tervo DG, Hwang BY, Viswanathan S, Gaj T, Lavzin M, Ritola KD, Lindo S, Michael S, Kuleshova E, Ojala D, Huang CC, Gerfen CR, Schiller J, Dudman JT, Hantman AW, Looger LL, Schaffer DV & Karpova AY (2016) A Designer AAV Variant Permits Efficient Retrograde Access to Projection Neurons. Neuron, 92, 372–382. [PubMed: 27720486]

Tordo J, O'Leary C, Antunes A, Palomar N, Aldrin-Kirk P, Basche M, Bennett A, D'Souza Z, Gleitz H, Godwin A, Holley RJ, Parker H, Liao AY, Rouse P, Youshani AS, Dridi L, Martins C, Levade T, Stacey KB, Davis DM, Dyer A, Clement N, Bjorklund T, Ali RR, Agbandje-McKenna M, Rahim AA, Pshezhetsky A, Waddington SN, Linden RM, Bigger BW & Henckaerts E (2018) A novel adeno-associated virus capsid with enhanced neurotropism corrects a lysosomal transmembrane enzyme deficiency. Brain, 141, 2014–2031. [PubMed: 29788236]

Weiss AR, Liguore WA, Domire JS, Button D & McBride JL (2020) Intra-striatal AAV2.retro administration leads to extensive retrograde transport in the rhesus macaque brain: implications for disease modeling and therapeutic development. Sci. Rep, 10, 6970. [PubMed: 32332773]

Wickersham IR, Finke S, Conzelmann KK & Callaway EM (2007) Retrograde neuronal tracing with a deletion-mutant rabies virus. Nat. Methods, 4, 47–49. [PubMed: 17179932]

Yamaguchi T, Wang HL & Morales M (2013) Glutamate neurons in the substantia nigra compacta and retrorubral field. Eur. J. Neurosci, 38, 3602–3610. [PubMed: 24102658]

Yeterian EH & Pandya DN (1998) Corticostriatal connections of the superior temporal region in rhesus monkeys. J. Comp. Neurol, 399, 384–402. [PubMed: 9733085]

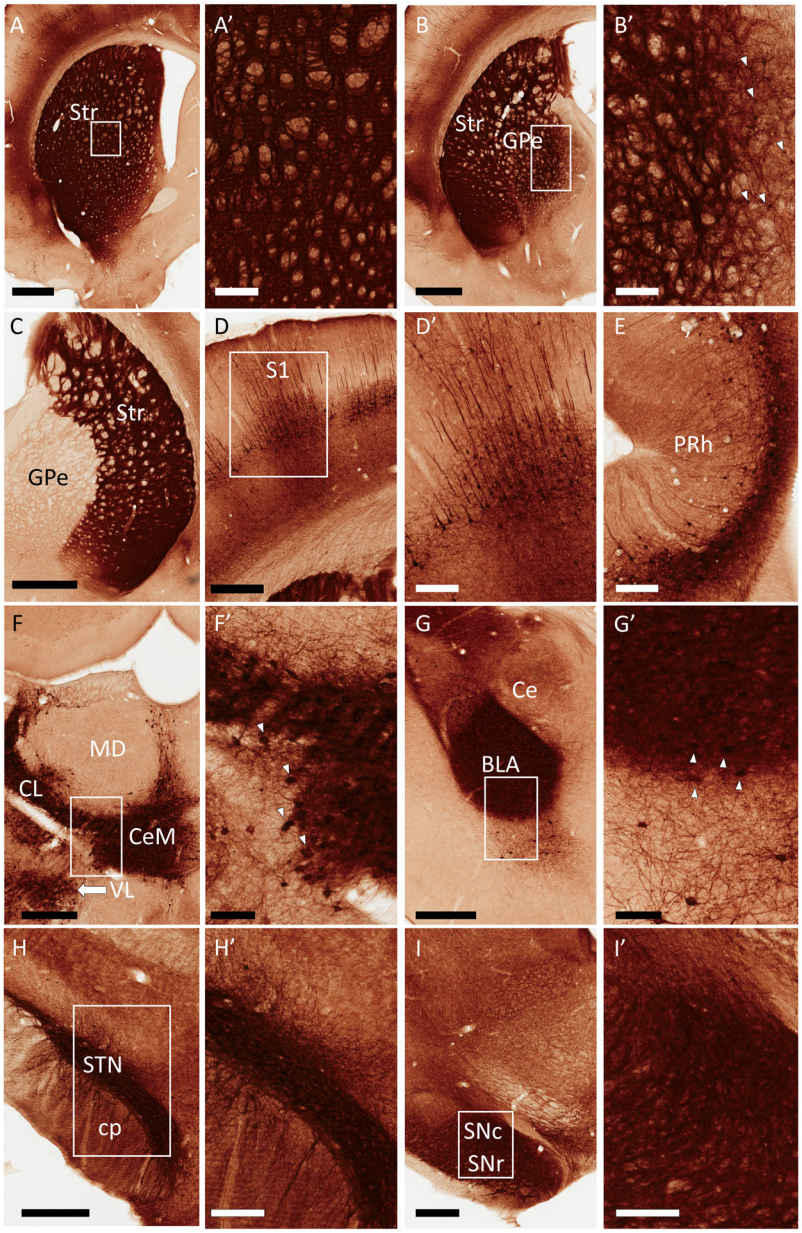

Figure 1:

Representative light micrographs of GFP expression in rat brain following a unilateral, intra-striatal injection of rAAV2-retro-hSyn-Jaws-GFP. All regions shown are from the hemisphere ipsilateral to the virus injection, except where indicated. Areas in rectangles are shown at higher magnification in the corresponding panels labeled with prime symbols. (**A**) Striatum (Str), (**B**) External globus pallidus (GPe), (**C**) GPe, contralateral side, (**D**) Ipsilateral primary somatosensory cortex (S1), (**E**) Perirhinal cortex (PRh), (**F**) Thalamus, (**G**) Amygdala, (**H**) Subthalamic nucleus (STN), (**I**) Substantia nigra. Additional abbreviations: basolateral amygdala (BLA), central amygdala (Ce), centrolateral thalamus (CL), central medial thalamus (CeM), cerebral peduncle (cp), mediodorsal thalamus (MD), substantia nigra pars reticulata (SNr), substantia nigra pars compacta (SNc), ventrolateral

thalamus (VL). Arrowheads in **B'**, **F'** and **G'** point to subsets of GFP+ cell bodies visible in these panels. GFP+ cells were also numerous in the STN, and also present in the SNc, although the intensity of neuropil labeling in these regions rendered such cell bodies difficult to display by these peroxidase images (see Figs. 3 and 4 for evidence of cell labeling in the rat SNc and STN, respectively). Scale Bars: 1mm (**A**, **B**, **C**); 500μm (**D**, **G**, **H**, **I**); 300μm (**F**); 200μm (**A'**, **B'**, **D'**, **E**, **H'**, **I'**); 100μm (**F'**, **G'**). Approximate rostrocaudal coordinates of sections, according to (Paxinos & Watson, 2006) in mm relative to Bregma: 1.2 (**A**); −0.84 (**B**, **C**, **D**); −4.44 (**E**); −2.52 (**F**); −3.36 (**G**); −3.6 (**H**); −6.12 (**I**). Figure includes micrographs from all 3 rats used in this study.

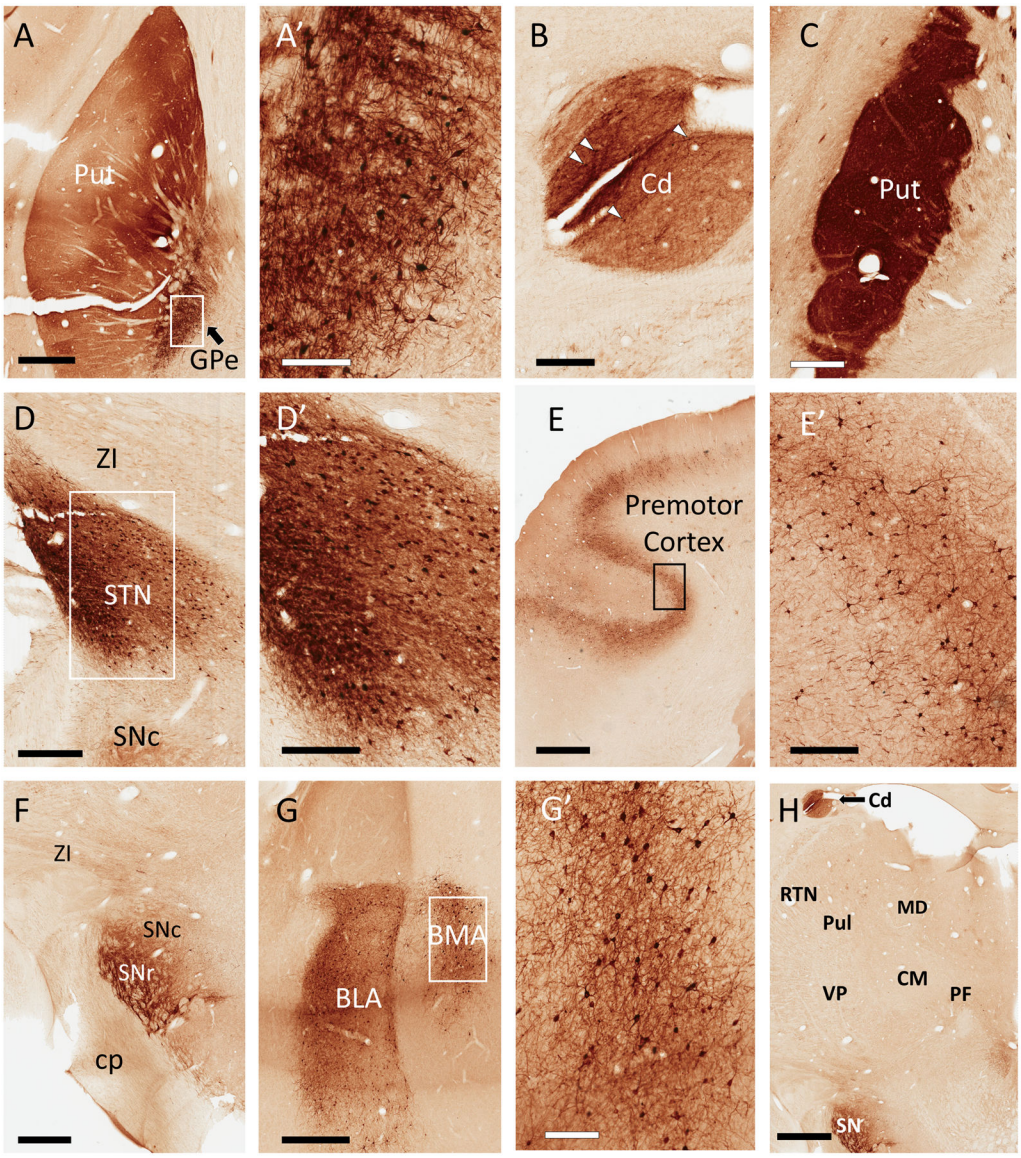

Figure 2:

Representative light micrographs of GFP expression in monkey brain following a unilateral, intra-striatal (putamen) injection of rAAV2-retro-hSyn-Jaws-GFP. All regions described below were ipsilateral to injection site. In the putamen (Put), neuropil was diffusely labeled, with scattered GFP+ cell bodies, particularly in the ventral territory (**A**). In the same section, numerous GFP+ cell bodies were found in the external globus pallidus (GPe) (**A** and **A'**). Similar to the Put, GFP+ fiber staining was observed in the caudate (Cd) (**B**; note that this section of caudate is also visible in Panel **H**). Similar to the rat striatum, the neuropil of the Put was densely labeled across the rostrocaudal axis, many millimeters away from the injection site (**C**). The subthalamic nucleus (STN) contained numerous GFP+ cell bodies and dense neuropil staining (**D** and **D'**). Varying numbers of deep-layer pyramidal cells were labeled in many cortical regions, including the premotor cortex (**E**, **E'**). In the substantia nigra, we observed GFP+ fibers, as well as a few labeled cell bodies bordering the compacta

(SNc) and reticulata (SNr) territories (**F**). Numerous GFP+ cells were located in the basolateral and basomedial amygdala (BLA and BMA, respectively) (**G** and **G'**). Remarkably, the thalamus was nearly devoid of GFP labeling (**H**). Additional abbreviations: centromedian nucleus of thalamus (CM), parafascicular nucleus of thalamus (PF), pulvinar (Pul), thalamic reticular nucleus (RTN), ventral posterior nucleus of thalamus (VP), zona incerta (ZI), all other abbreviations as described in Figure 1. Scale Bars: 2mm (**E**, **H**) 1mm (**A**, **F**, **G**); 600μm (**C**); 500μm (**D**); 300μm (**B**, **D'**, **E'**); 200μm (**A'**, **G'**). Approximate rostrocaudal coordinates of sections, according to (Paxinos *et al.*, 1999) in mm relative to interaural line: 10.2 (**A**, **D**); 7.5 (**B**, **C**, **F**, **H**); 19.65 (**E**); 14.7 (**G**). Figure includes micrographs from both monkeys used in this study.

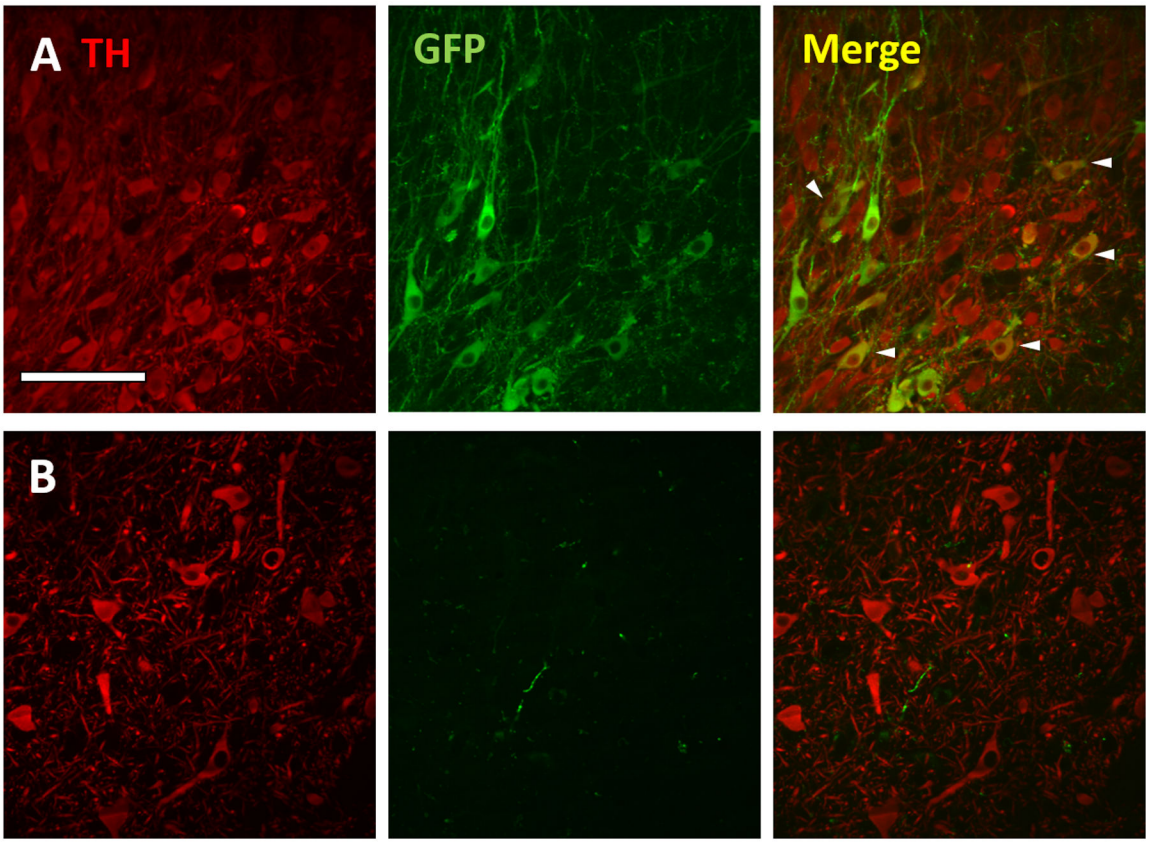

Figure 3:

GFP expression in dopaminergic (tyrosine hydroxylase (TH)-positive) neurons in the rat, but not monkey SNc following intra-striatal rAAV2-retro injection. Confocal images of TH (red; left), GFP (green; middle) and merged markers (right) of the rat (row **A**) and monkey (row **B**). SNc ipsilateral to injection site. Arrowheads in merged image depict a subset of GFP +/TH+ cells (yellow) in the rat SNc. Scale bar: 100μm.

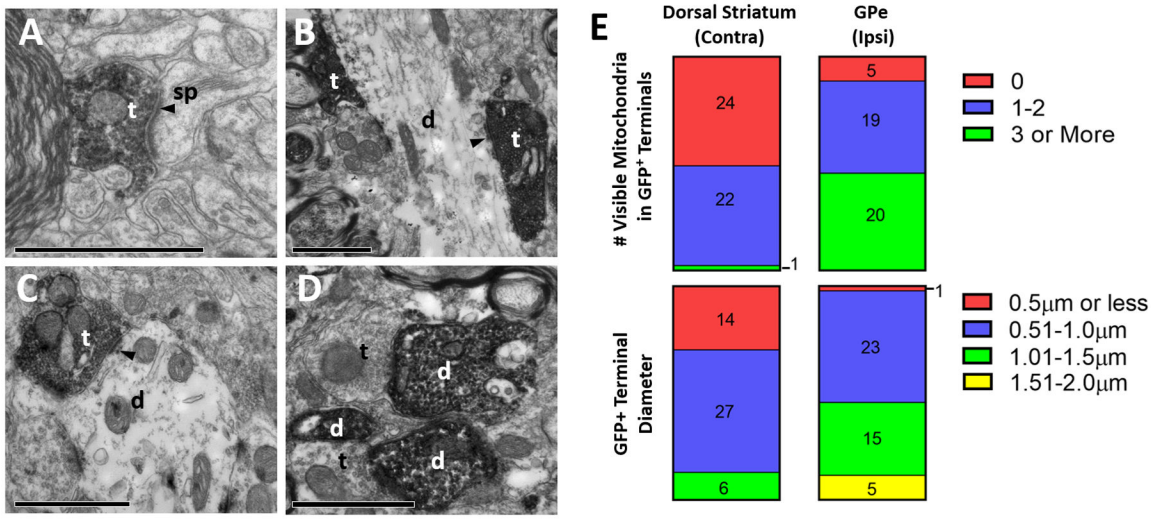

Figure 4:

Ultrastructural analysis of GFP-positive elements in the rat basal ganglia, after intra-striatal injection of rAAV2-retro-hSyn-Jaws-GFP. **A**-**D**: Representative electron micrographs of GFP-immunopositive elements (revealed with peroxidase). (**A**) GFP-labeled axonal terminal in striatum contralateral to the injection site, (**B**) labeled terminals in GPe ipsilateral to the injection site, (**C**-**D**) labeled terminal and dendrites in ipsilateral STN. Abbreviations: t (axon terminal), d (dendrite), sp (spine). White or black text for these abbreviations indicate if the element is GFP-positive or negative, respectively. Arrowhead denotes asymmetric synapse made by labeled terminals. All scale bars: 1μm. (**E**) Quantification of diameter (top) and number of visible mitochondria inside immunolabeled terminals (bottom) in the contralateral striatum (left) and ipsilateral GPe (right). Numbers in bars refer to total terminal counts for each category.

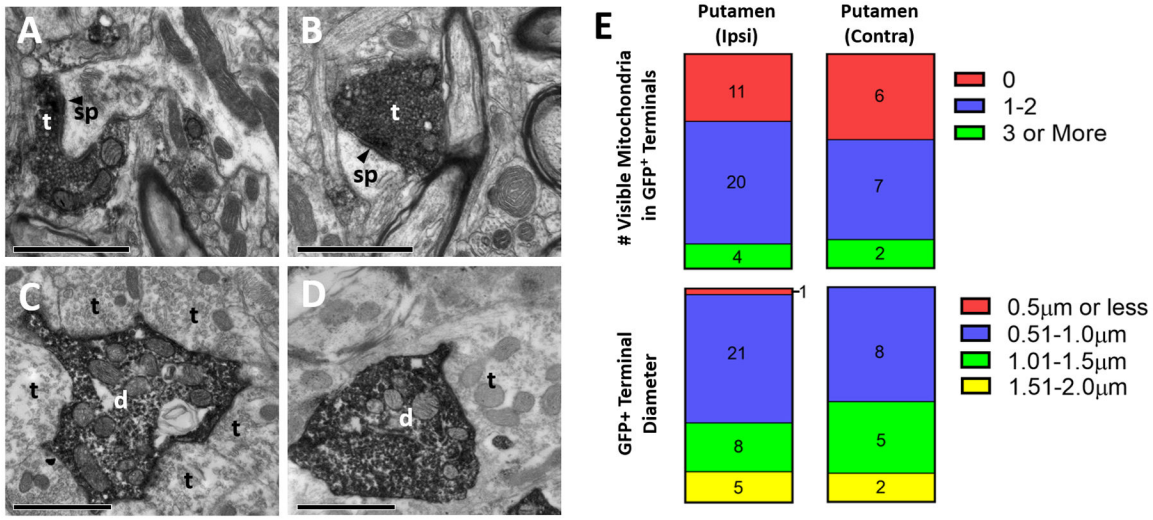

Figure 5:

Ultrastructural analysis of GFP-positive elements in the monkey basal ganglia after intra-striatal injection of rAAV2-retro-hSyn-Jaws-GFP. A-D: Representative electron micrographs of GFP-immunopositive elements (revealed with peroxidase). (**A**) GFP-positive terminal in putamen ipsilateral to injection site, (**B**) labeled terminal in putamen contralateral to injection site, (**C**) labeled dendrite in ipsilateral GPe, (**D**) labeled dendrite in ipsilateral STN. Abbreviations: t (axon terminal), d (dendrite), sp (spine). White or black text for these abbreviations indicate if the element is GFP-positive or negative, respectively. Arrowhead denotes asymmetric synapse made by labeled terminals. All scale bars: 1µm. (**E**) Quantification of diameter (top) and number of visible mitochondria inside immunolabeled terminals (bottom) in the ipsilateral (left) and contralateral (right) putamen. Numbers in bars refer to total terminal counts for each category.

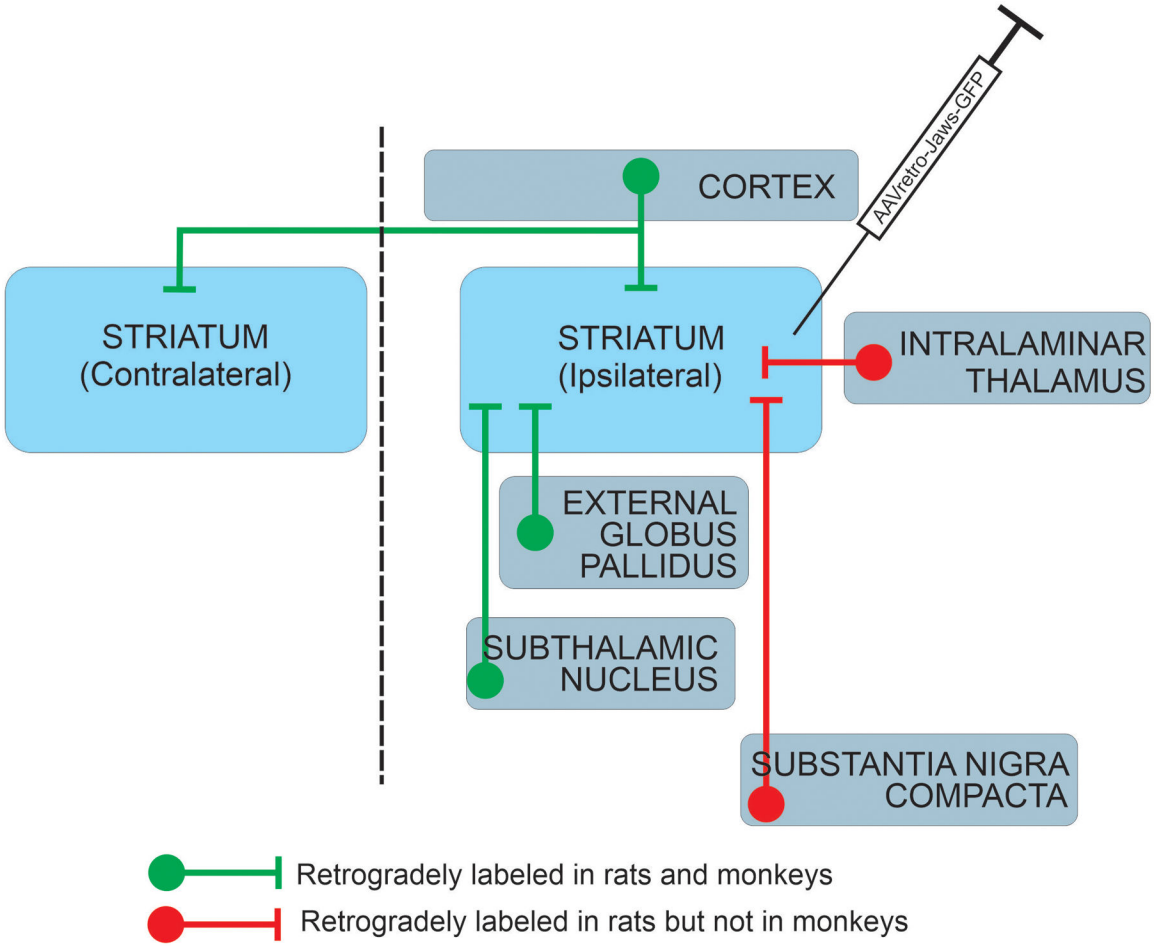

Figure 6:
Comparison of neuronal pathways transduced by intra-striatal rAAV2-retro injection in rat and monkey.